R2PS: Worst-Case Robust Real-Time Pursuit Strategies under Partial Observability

Runyu Lu[1,2]   Ruochuan Shi[2,1]   Yuanheng Zhu[2,1]   Dongbin Zhao[2,1]

[1] School of Artificial Intelligence, University of Chinese Academy of Sciences
[2] Institute of Automation, Chinese Academy of Sciences
lurunyu17@mails.ucas.ac.cn

November 24, 2025

Abstract

Computing worst-case robust strategies in pursuit-evasion games (PEGs) is time-consuming, especially when real-world factors like partial observability are considered. While important for general security purposes, real-time applicable pursuit strategies for graph-based PEGs are currently missing when the pursuers only have imperfect information about the evader's position. Although state-of-the-art reinforcement learning (RL) methods like Equilibrium Policy Generalization (EPG) and Grasper provide guidelines for learning graph neural network (GNN) policies robust to different game dynamics, they are restricted to the scenario of perfect information and do not take into account the possible case where the evader can predict the pursuers' actions. This paper introduces the first approach to worst-case robust real-time pursuit strategies (R2PS) under partial observability. We first prove that a traditional dynamic programming (DP) algorithm for solving Markov PEGs maintains optimality under the asynchronous moves by the evader. Then, we propose a belief preservation mechanism about the evader's possible positions, extending the DP pursuit strategies to a partially observable setting. Finally, we embed the belief preservation into the state-of-the-art EPG framework to finish our R2PS learning scheme, which leads to a real-time pursuer policy through cross-graph reinforcement learning against the asynchronous-move DP evasion strategies. After reinforcement learning, our policy achieves robust zero-shot generalization to unseen real-world graph structures and consistently outperforms the policy directly trained on the test graphs by the existing game RL approach.

1   Introduction

Pursuit-evasion game (PEG) is an important topic long examined in the fields of robotics and security (Vidal et al., 2001, 2002; Chung et al., 2011). Many real-world tasks can benefit from the solution to an abstracted PEG, e.g., guiding a team of cops to capture a robber and aligning a team of guards to defend against an intruder. In comparison with traditional differential games (Margellos & Lygeros, 2011; Zhou et al., 2012), graph-based PEGs are convenient for describing complicated scenarios, possibly with a large scale. When we use graphs as a common structural representation, the actions of the pursuers and the evader can be abstracted as moving from a vertex to an adjacent one at each discrete timestep. The edges between the vertices can possibly represent urban streets in reality.

However, exactly solving graph-based PEGs is computationally expensive (see Goldstein & Reingold (1995)). Even under a slight structural change, the worst-case robust pursuit strategies can be different and thus require a large amount of time to be recomputed. For example, when a traffic jam happens in the city, the related edges in the PEG graph can be frequently removed and added. This severely limits the real-time applicability of the existing methods featuring mathematical programming (Vieira et al., 2008; Horák & Bošanský, 2017). Besides, real-world factors like partial observability, which leads to PSPACE-hardness even under a fixed opponent (see Papadimitriou & Tsitsiklis (1987)), further increase the difficulty of deriving a well-performing pursuit strategy within a time limit.

Reinforcement learning (RL), which has demonstrated strong generalization capabilities in domains like large language models (see Chu et al. (2025)), provides an alternative solution to this problem. We may train a parameterized policy represented by a suitable neural network, e.g., a graph neural network (GNN) (Wu et al., 2020), on a diverse set of

graphs and then generalize it to the unseen graph structures. Unfortunately, while RL has been applied to solving large-scale PEGs (Xue et al., 2022, 2021), existing research focuses more on its scalability rather than generalization capability. The methods like MT-PSRO (Li et al., 2023) and Grasper (Li et al., 2024) are limited to few-shot generalization to unseen opponent strategies and initial conditions. As is pointed out by Zhuang et al. (2025), they still have difficulty adapting to rapid changes of graph structures. The state-of-the-art method, Equilibrium Policy Generalization (EPG) (Lu et al., 2025a), first examines zero-shot generalization at the level of graphs. However, whether the paradigm of EPG works under partial observability remains underexplored. Besides, all of the mentioned works do not consider the possible case that the evader may have stronger observation capabilities than the pursuers. This makes the strength of the learned pursuit strategies less convincing for real-world security purposes.

In this paper, we present an approach to finding pursuit strategies that are both worst-case robust and real-time applicable under partial observability. We start by analyzing a dynamic programming (DP) algorithm for efficiently solving Markov PEGs and proving that it also finds optimal strategies when the evader can predict the pursuer's action and move asynchronously. With a belief update mechanism, we further extend the DP policies to a partially observable setting. The belief preservation serves to avoid the complexity of recording all observation histories through abstracting opponent information for effective decision-making. Finally, we embed the belief preservation mechanism into the reinforcement learning framework of EPG and train a generalized GNN pursuer policy under partial observability. Following the principle of EPG, the training proceeds in a diverse set of graphs against the provably optimal DP evader. We then evaluate the worst-case robustness of our real-time RL pursuer policy under unseen real-world graph structures.

Specifically, the contributions of this paper are three threefold:

- We theoretically analyze a dynamic programming (DP) algorithm and extend the optimal strategies induced by this algorithm to asynchronous-move and partially observable scenarios. We prove that the DP algorithm induces strictly optimal pursuit and evasion strategies when the evader moves asynchronously and design a belief preservation mechanism against the possibly unobserved evaders. Under belief preservation, we verify that the extended pursuer policy remains strong against the provably optimal perfect-information evader.

- We practically train an observation-based pursuer policy across different graph structures, deriving the first worst-case robust real-time pursuit strategies (R2PS) applicable to dynamically changing PEGs with partial observations. We combine our belief preservation mechanism with the state-of-the-art robust policy generalization paradigm, EPG, and provide an inference time complexity bound for our GNN-represented RL pursuer policy.

- Through extensive experiments, we verify that under partial observability, our RL training against the asynchronous-move DP evaders under a diverse set of graphs leads to robust zero-shot performance in unseen real-world graphs. Comparative results reveal the superiority of our approach over the standard game RL approach, PSRO (Lanctot et al., 2017), even against a best-responding evader. Additionally, we confirm that our RL policy scales effectively with more complex real-world graphs and that the pursuit performance can benefit from our belief updates and be enhanced by increased observation ranges.

2 Preliminaries

2.1 Problem Formulation

Adversarial games with partial observability can be generally represented by partially observable stochastic games (POSGs), where equilibrium learning has been rigorously examined in existing game-theoretic research (e.g., Lu et al. (2025b)). However, this formulation considers all possible observation histories and leads to a large set of decision points whose size is possibly exponential in the time horizon of the game. For the worst scenario of pursuit-evasion, while the pursuers have limited observation capabilities, the evader could still obtain the global information of the game. Since at least one side of the players possesses perfect information, it is less efficient to formulate PEGs as complete POSGs. Therefore, in order to avoid the inherent PSPACE-hardness from the problem formulation, we consider first expressing PEGs as two-player zero-sum Markov games and then extending the definitions to incorporate practical adversarial factors like partial observability and asynchronous moves of the evader. The ultimate goal is to adjust the efficient algorithms for solving Markov PEGs to the imperfect-information setting with little sacrifice of robustness.

Two-player zero-sum Markov game. An infinite-horizon two-player zero-sum Markov game is represented by a tuple $(S, \mathcal{A}, \mathcal{B}, \mathcal{P}, r, \gamma)$, where S is the state space, $\mathcal{A}$ is the action space of the max-player (who aims to maximize the cumulative reward), $\mathcal{B}$ is the action space of the min-player (who aims to minimize the cumulative reward),

$\mathcal{P} \in [0,1]^{|S||\mathcal{A}||\mathcal{B}| \times |S|}$ is the transition probability matrix, $r \in [0,1]^{|S||\mathcal{A}||\mathcal{B}|}$ is the reward vector, and $\gamma \in (0,1)$ is the discount factor. In PEGs, the max-player is the team of m pursuers, and the min-player is the evader. We use a termination function $f : S \to \{0,1\}$ to mark the states where the pursuit is successful. When $f(s) = 1$, the game is terminated, and a reward of $+1$ is received. Otherwise, a reward of 0 is received. The discount factor $\gamma < 1$ encourages the pursuers to capture the evader as soon as possible.

Graph-based pursuit-evasion game. Considering the requirements of formulating large-scale real-world scenarios, we describe states and actions on a graph structure $G = \langle \mathcal{V}, E \rangle$: $\mathcal{V}$ is the set of vertices v. The global state $s = (s_p, s_e)$ in a game is an element of $\mathcal{V}^m \times \mathcal{V}$, where $s_p = (v_p^1, v_p^2, \cdots, v_p^m) \in \mathcal{V}^m$, and $s_e = v_e \in \mathcal{V}$. An edge $e = (v, v') \in E$ defines the adjacency between two vertices $v, v' \in \mathcal{V}$. For example, when we represent an urban scenario by a graph G, an edge e can be used to describe a unit length of streets. The valid actions of the $m + 1$ agents in a graph-based PEG are either moving to an adjacent vertex via an edge or staying at the current node.

Policy and value function. Following common notations, we denote by (μ, ν) the joint policy of the two players, where μ is the policy of the max-player (pursuers) and ν is the policy of the min-player (evader): $\mu(s) \in \Delta(\mathcal{A})$ (resp., $\nu(s) \in \Delta(\mathcal{B})$) is the max-player's (resp., min-player's) action distribution at state $s \in S$. Since $\Delta(\mathcal{A})$ is the probability simplex over $\mathcal{A}$, $\mu(s,a)$ corresponds to the probability of selecting action $a \in \mathcal{A}$ at state s. Given the joint policy, we further define the value function $V^{\mu,\nu}(s) = \mathbb{E}\left[\sum_{t=0}^{\infty} \gamma^t r(s_t, a_t, b_t) | s_0 = s; \mu, \nu\right]$ as in Markov decision processes.

Solution concept. A Nash equilibrium (NE) in a game is a joint policy where each individual player cannot benefit from unilaterally deviating from his/her own policy (Roughgarden, 2016). Specifically, in a two-player zero-sum MG, an NE (μ^*, ν^*) satisfies $V^{\mu,\nu^*} \leq V^{\mu^*,\nu^*} \leq V^{\mu^*,\nu}$ for any μ and ν at all states. As is well known, every MG with finite states and actions has at least one NE, and all NEs in a two-player zero-sum MG share the same value $V^*(s) = V^{\mu^*,\nu^*}(s) = \max_\mu \min_\nu V^{\mu,\nu}(s) = \min_\nu \max_\mu V^{\mu,\nu}(s)$ (Shapley, 1953). In two-player zero-sum Markov games, Nash equilibrium can be viewed as a globally optimal joint policy since both players cannot be exploited by their worst-case opponents when the players move synchronously (simultaneously).

Game extension. Since Markov games only take into account synchronous moves and full observations, we further allow for two variations concerning asynchronous moves and partial observability. In reality, the worst evader (from the pursuers' perspective) may have good predictions of the pursuit actions. Therefore, we allow it to decide after the pursuers' move a at each timestep. In this case, the evader policy $\nu(s)$ is transformed into an asynchronous one $\nu(s,a)$, and we say that a strategy is optimal for the pursuer/evader side at state s if the worst-case termination timesteps of all possible trajectories starting from s are maximized/minimized. Besides, the availability of sensors may not allow the pursuers to observe an agent that is far away (while the worst evader can). In this case, the pursuer policy $\mu(s)$ is transformed into $\mu(o)$, where o is the history of the pursuers' local observations.

2.2 Dynamic Programming for Markov PEGs

The traditional marking algorithm (Chung et al., 2011) provides a general idea of recursively finding optimal strategies in perfect-information PEGs. If all possible evading actions lead to the states that have been marked, then we can also mark the current state, which means the pursuers can capture the evader starting from this state. However, a direct implementation of the marking algorithm incurs a time complexity much higher than the theoretical lower bound $\Omega(|S|)$. In view of this gap, Lu et al. (2025a) introduce a dynamic programming (DP) algorithm (see Algorithm 1) that guarantees near-optimal time complexity for solving Markov PEGs.

Algorithm 1 computes a distance table D through preserving a queue $\mathcal{Q}$. Intuitively, the distance value $D(s)$ indicates the worst-case timestep for the pursuer side to capture the evader starting from the global state $s = (s_p, s_e)$, which is guaranteed through the use of a minimax policy

$$\mu^*(s_p, s_e) = \underset{\text{neighbor } n_p \text{ of } s_p}{\arg\min} \left\{ \max_{\text{neighbor } n_e \text{ of } s_e} D(n_p, n_e) \right\}. \tag{1}$$

Under synchronous moves, the evader's policy is symmetrically defined as

$$\nu^*(s_p, s_e) = \underset{\text{neighbor } n_e \text{ of } s_e}{\arg\max} \left\{ \min_{\text{neighbor } n_p \text{ of } s_p} D(n_p, n_e) \right\}. \tag{2}$$

Using mathematical induction, Lu et al. (2025a) prove that the joint policy (μ^*, ν^*) is a near-optimal pure strategy (the proof can be found in Appendix A.1):

Theorem 1. *If there exists a pure-strategy Nash equilibrium in the Markov PEG, then the joint policy (μ^*, ν^*) defined by (1) and (2) is a Nash equilibrium.*

Algorithm 1: Dynamic Programming for Markov PEGs

Input: Graph $G = \langle \mathcal{V}, E \rangle$, Pursuer Number m, and Termination Function $f : \mathcal{V}^m \times \mathcal{V} \to \{0, 1\}$

1 Initialize an empty queue $\mathcal{Q}$ and the distance table $D = \infty$

2 for *pursuer state (positions)* $s_p \in \mathcal{V}^m$ **do**

3   **for** *evader state* $s_e \in \mathcal{V}$ **do**

4   **if** $f(s_p, s_e) = 1$ **then**

5 $D(s_p, s_e) \leftarrow 0$

6   Push (s_p, s_e) into $\mathcal{Q}$

7   **end**

8   **end**

9 end

10 while $\mathcal{Q}$ *is not empty* **do**

11   Pop the first element (s_p, s_e) from $\mathcal{Q}$

12   **for** *evader neighbor* $n_e \in \text{Neighbor}(s_e), \nexists n_e' \in \mathcal{V}, (n_e, n_e') \in E, D(s_p, n_e') > D(s_p, s_e)$ **do**

13   **for** *pursuer neighbor* $n_p \in \text{Neighbor}(s_p) \subset \mathcal{V}^m, D(n_p, n_e) = \infty$ **do**

14 $D(n_p, n_e) \leftarrow D(s_p, s_e) + 1$

15   Push (n_p, n_e) into $\mathcal{Q}$

16   **end**

17   **end**

18 end

Output: Distance Table D

---

3 Extending Dynamic Programming Policies to Asynchronous Moves and Partial Observability

In this section, we further show that the distance table D generated by the DP algorithm (Algorithm 1) can also be used to construct the optimal evader policy under asynchronous moves, as well as the observation-based pursuer policies under partial observability.

3.1 Asynchronous-Move Setting

When the evader moves asynchronously, we define the DP policy for the evader as

$$\nu^*(s_p, s_e, n_p) = \underset{\text{neighbor } n_e \text{ of } s_e}{\arg\max} \{D(n_p, n_e)\}, \tag{3}$$

where n_p is the neighbor of s_p that the pursuers choose to move to in the current decision step, which is perceived or predicted by the evader in advance. With this information as an additional input, the evader can decide based on the pursuers' positions after their decision rather than before. As a result, the policy (3) no longer requires the inner enumeration in (2).

In this case, we can show that the pursuer policy (1) and evader policy (3) induced by the distance table D are strictly optimal at all states. We start our analysis by proving Lemma 1, which reveals the minimax essence of the distance table D. The detailed proof can be found in Appendix A.2.

Lemma 1. *When $D(n_p, n_e) > 0$, Algorithm 1 guarantees that*

$$D(n_p, n_e) = \underset{\text{neighbor } s_p \text{ of } n_p}{\min} \left\{ \underset{\text{neighbor } s_e \text{ of } n_e}{\max} D(s_p, s_e) \right\} + 1.$$

Using Lemma 1, we can further prove that $D(s)$ implies the best possible worst-case timesteps starting from state s for both pursuer and evader sides under the asynchronous-move setting. The main results are shown as follows, and the omitted proofs can be found in Appendix A.3-A.5.

Theorem 2. *Starting from any state $s = (s_p, s_e)$ satisfying $D(s) = d < \infty$, μ^* guarantees pursuit within d steps against any evasion strategy, and ν^* avoids being captured in less than d steps by any pursuit strategy.*

Based on the definition of optimal strategies in the asynchronous-move setting (see Section 2.1), Theorem 2 directly implies the following corollary:

Corollary 1. *For any state $s = (s_p, s_e)$ with $D(s) < \infty$, both μ^* and ν^* are optimal strategies.*

Furthermore, we use Theorem 3 to show that whether m perfect-information pursuers are sufficient to capture the evader starting from state s can be determined by whether $D(s) < \infty$:

Theorem 3. *Starting from any state $s = (s_p, s_e)$ with $D(s) = \infty$, ν^* can never be captured by any pursuit strategy.*

3.2 Partially Observable Setting

Since the DP algorithm provably generates optimal strategies when both pursuer and evader sides have full observations, it is appealing to reuse the distance table D to construct a pursuit strategy under partial observability for real-world security purposes. We expect that the observation-based pursuer policy, which is extended from the DP policy under perfect information, should effectively extract history information and align with the original policy when the observation range is infinity.

We consider the following partially observable setting for the pursuers, who may serve as guards in a large area. The PEG begins because an intruder is observed, whose initial position is revealed to the pursuers. Once the game starts, the position of the evader (intruder) can no longer be detected unless it is in the observation range of at least one pursuer. For example, setting the observation range to be 2 means that the evader can be detected only when its distance to one pursuer is less than 3.

Under the partially observable setting, the observation history o induces the possible positions of the evader, which we denote by a set Pos. This set is initialized as $\{s_e\}$, where s_e is the initial position of the evader. As the game proceeds, it is updated based on the pursuers' observations at each timestep:

$$\text{Pos}_{\text{new}} = \begin{cases} \{s_e\} & \text{evader is observed at } s_e, \\ \text{Remove}(\text{Neighbor}(\text{Pos}_{\text{old}})) & \text{evader is not observed.} \end{cases} \tag{4}$$

where the operator $\text{Remove}(\cdot)$ excludes all currently observed positions (since the evader is currently unobserved) from the possible evader positions represented by $\text{Neighbor}(\text{Pos}_{\text{old}})$, which corresponds to the set of one-step neighbors of the nodes in Pos_{old}.

Given Pos, we can express $\mu(o)$ as $\mu(s_p, \text{Pos})$ and construct a minimax policy that bounds the worst-case pursuit timesteps if we assume that the pursuers resume full observability after this step:

$$\mu(s_p, \text{Pos}) = \operatorname*{arg\,min}_{\text{neighbor } n_p \text{ of } s_p} \left\{ \max_{s_e \in \text{Pos}} \max_{\text{neighbor } n_e \text{ of } s_e} D(n_p, n_e) \right\}$$

$$= \operatorname*{arg\,min}_{\text{neighbor } n_p \text{ of } s_p} \left\{ \max_{n_e \in \text{Neighbor}(\text{Pos})} D(n_p, n_e) \right\}. \tag{5}$$

While this policy is applicable to the case of partial observability, it is based on an assumption that the observation limitation is not continual. Under continual partial observability, we find that averaging the timesteps through preserving a **belief** about the evader's position can further encourage effective pursuit, especially when the set Pos is large. The belief-averaged pursuer policy is expressed as

$$\mu(s_p, \text{belief}) = \operatorname*{arg\,min}_{\text{neighbor } n_p \text{ of } s_p} \left\{ \frac{\sum_{s_e} \text{belief}(s_e) \max_{\text{neighbor } n_e \text{ of } s_e} D(n_p, n_e)}{\sum_{s_e} \text{belief}(s_e)} \right\}, \tag{6}$$

where the belief function is initialized to be 0 except for the initial evader position and updated by

$$\text{belief}_{\text{new}}(s_e) \leftarrow \begin{cases} 0 & s_e \notin \text{Pos}, \\ \sum_{\text{neighbor } v \text{ of } s_e} \nu(v, s_e) \text{belief}_{\text{old}}(v) & s_e \in \text{Pos}. \end{cases} \tag{7}$$

Since the pursuer side cannot obtain the evader's policy ν when no prior knowledge is available, $\nu(v)$ is set to be a uniform distribution over $\text{Neighbor}(v)$ by default.

As the original DP policy $\mu^*(s)$ is provably optimal, Lemma 2 guarantees that both the position-extended policy $\mu(s_p, \text{Pos})$ and the belief-averaged policy $\mu(s_p, \text{belief})$ maintain the pursuit optimality when there is unlimited observation capability. The proof can be found in Appendix A.6.

Lemma 2. *When* Pos *is always a singleton, both pursuer policies (5) and (6) will be reduced to their perfect-information counterpart (1).*

Note that the time complexity of preserving Pos and belief is only $\tilde{\mathcal{O}}(|\mathcal{V}|)$ at each timestep, where $\tilde{\mathcal{O}}$ hides the additional factor of enumerating the neighbors. Since the average degree in the real-world graphs can be small (see Table 1 in Section 5), the computation is practically efficient. In Appendix B, we provide the illustrations of the belief preservation process for a more intuitive understanding.

4 Finding Robust Real-Time Pursuit Strategies (R2PS) via Adversarial Reinforcement Learning across Graphs

4.1 Adversarial Reinforcement Learning

Since the DP algorithm has a lower-bound time complexity exponential in the agent number, it can be impractical to directly apply the DP policies in real time when the graph structure of the game dynamically changes. In view of this problem, we further combine our belief preservation mechanism with the idea of Equilibrium Policy Generalization (EPG) (Lu et al., 2025a) to construct a reinforcement learning method, which makes use of some preprocessed D tables and the induced policies to train a generalized pursuer policy across a diverse set of graphs. We use the cross-graph RL policy for zero-shot generalization under unseen graph structures, aiming to derive worst-case robust real-time pursuit strategies (R2PS) under partial observability.
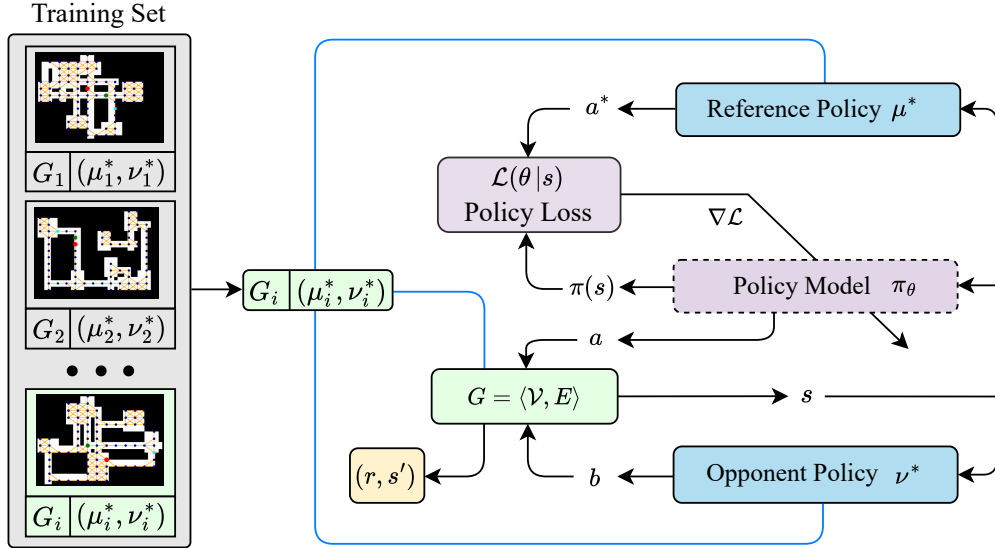

Figure 1: Cross-Graph Reinforcement Learning of Generalized Pursuer Policy

Figure 1 illustrates the cross-graph reinforcement learning pipeline, which features unexploitable evader policies as adversaries. The training set contains graphs with various topologies G_i and the DP policies (μ_i^*, ν_i^*) induced by the preprocessed D tables. In each iteration, a graph G_i along with the policy (μ_i^*, ν_i^*) is sampled. Under graph $G = G_i$, we use $\mu^* = \mu_i^*$ as the reference policy to guide policy training and use $\nu^* = \nu_i^*$ as the adversarial policy. Following the principle of EPG, we train a cross-graph pursuer policy through reinforcement learning against ν^* with the guidance of μ^*.

Specifically, for a transition (s, a, b, r, s') in the replay buffer: s is a randomly generated global state in the sampled graph; a is the pursuers' joint action sampled from the current policy model π_θ, which is ideally a graph neural network (Wu et al., 2020) with parameter θ that enables real-time inference; b is the evader's action generated from

the asynchronous-move opponent policy ν^* (3); the instant reward r and the next state s' are generated by the PEG dynamics under graph structure $G = \langle \mathcal{V}, E \rangle$.

Given state s, the reference policy μ^* generates a deterministic reference action $a^* = \mu^*(s)$ and serves to construct the policy loss

$$\mathcal{L}\left(\theta\,|\,s\right) = J_\pi(\theta\,|\,s) + \beta D_{\mathrm{KL}}\left(\mu^*(s), \pi(s)\right) = J_\pi(\theta\,|\,s) - \beta \log \pi_\theta(s, a^*), \tag{8}$$

where $J_\pi(\theta\,|\,s)$ is the original policy loss of any backbone (multi-agent) reinforcement learning algorithm (e.g., MAPPO (Yu et al., 2022)), and β is a hyperparameter that balances policy guidance (for efficient exploration) and reinforcement learning loss (for policy optimization).

When training pursuers under partial observability, we transform the input of the policy model π_θ by

$$s \leftarrow (s_p, \mathrm{Pos}, \mathrm{belief})$$

and use the observation-based policy $\mu(s_p, \mathrm{Pos})$ (5) or $\mu(s_p, \mathrm{belief})$ (6) to replace $\mu^*(s)$ (1), where Pos and belief are the preserved evader information under partial observability.

For dynamic games like PEGs, the policy space has certain transitivity structures. Czarnecki et al. (2020) show that the strategies in real-world games have different levels of transitive strength, with Nash equilibrium being the strongest. In a single-graph PEG, reinforcement learning against the optimal evader policy ν^* helps to exclude the pursuer policies that are transitively weaker. Cross-graph training is similar to finding the joint part of the remaining strategies and abstracting them to a worst-case robust policy under a diverse set of graph structures, where the divisions on the policy space through adversarial RL can be different. Imagine that a half space is excluded after each single-graph division and that the division criteria of different graphs are independent due to structural distinctions. In this ideal case, the cross-graph policy will be improved at an exponential level across a diverse training corpus, leading to robust pursuit strategies even under partial observability.

4.2   Implementation and Complexity Analysis

Technically, we use soft-actor critic (SAC) (Haarnoja et al., 2018; Christodoulou, 2019) as the backbone RL algorithm and employ a decentralized architecture with a parameter-sharing graph neural network (GNN) (Cao et al., 2023; Lu et al., 2025a) to represent the graph-based policy of the homogeneous pursuers. The SAC algorithm features a self-adaptive entropy regularization that balances exploration and exploitation, with double Q-learning (Hasselt, 2010) employed to avoid overestimation. The GNN architecture combines multi-head self-attention (Vaswani et al., 2017) with adjacent-matrix masks to encode graph-based states. The state embedding is then sent into a decoder followed by a pointer network (Vinyals et al., 2015) for graph-based policy output.

The implementation details and hyperparameter setting are reserved in Appendix C to save space. According to the corresponding analysis, the overall time complexity of computing the graph-based state feature is $\mathcal{O}(n^2 m)$, where $n = |\mathcal{V}|$ is the number of vertices in the graph, and m is the number of pursuers. Since the complexity of GNN queries is also $\mathcal{O}(n^2 m)$, and the complexity of preserving Pos and belief is $\tilde{\mathcal{O}}(n)$, the overall inference time complexity of the RL pursuer policy at each timestep is only $\mathcal{O}(n^2 m) + \mathcal{O}(n^2 m) + \tilde{\mathcal{O}}(n) = \mathcal{O}(n^2 m)$. In comparison, the time complexity of recomputing DP policies is $\tilde{\mathcal{O}}(n^{m+1})$ under dynamically changing graph structures (see Lu et al. (2025a)), as Algorithm 1 needs to be repeatedly executed. Here we briefly show the inference time gap arising from this complexity distinction. When $n = 1000$ and $m = 2$, it takes over 2 minutes to run Algorithm 1 at each timestep using an Intel Core i9-13900HX CPU. The inference time of our GNN-represented RL policy, however, is less than 1 second under the same condition. Our subsequent tests further show this inference can be reduced to below 0.01 seconds under GPU accelerations.

5   Evaluations

Here we provide our experimental evaluations of single-graph DP pursuers and cross-graph RL pursuers under partial observability. We assume that there are two pursuers ($m = 2$) against the single evader. This is a reasonable setting in view of the graph-theoretic result that 3 pursuers with full observations can always capture the evader in any planar graph (Fromme & Aigner, 1984). The initial position is randomly generated under the restriction that the distance between the evader and the pursuers is larger than the observation range of 2. Besides, no observation sensors except

for the pursuers themselves are allowed. The test graphs include Grid Map (a 10×10 grid), Scotland-Yard Map (from the board game Scotland-Yard), Downtown Map (a real-world location from Google Maps), and 7 famous real-world spots (from Times Square to Sydney Opera House). The graph details are shown in Appendix D.1, and the statistics of these graphs are shown in Table 1 (left).

Table 1: Graph Data (Total Node Number, Average Degree, Diameter) and Success Rate Comparison

	Node	Degree	Diameter	Shortest Path	DP_{Pos}	DP_{belief}
Grid Map	100	3.60	18	0.00	0.59	**0.78**
Scotland-Yard Map	200	3.91	19	0.00	0.44	**0.63**
Downtown Map	206	2.98	19	0.02	0.73	**0.90**
Times Square	171	2.58	22	0.01	0.41	**0.69**
Hollywood Walk of Fame	201	2.42	31	0.01	0.25	**0.48**
Sagrada Familia	231	2.60	25	0.00	0.24	**0.36**
The Bund	200	2.53	29	0.03	0.30	**0.57**
Eiffel Tower	202	2.34	38	0.29	0.69	**0.94**
Big Ben	192	2.48	34	0.08	0.54	**0.74**
Sydney Opera House	183	2.33	37	0.05	0.47	**0.87**

5.1 Evaluations of Extended DP Pursuers

We first evaluate the strength of the extended DP pursuers under partial observability (Section 3.2). We denote by DP_{Pos} the position-extended pursuer (5) and by DP_{belief} the belief-averaged pursuer (6). The pursuers succeed ($f(s) = 1$) when at least one of them is adjacent to the evader on the graph within 128 timesteps, and the success rates are averaged over 500 tests. To simulate the difficult case for security purposes, the evader is set to be the provably optimal DP evader (3) with global observations and asynchronous moves. For an intuitive comparison, we also include the result of directly following the shortest path to the evader under full observability.

As is shown in Table 1 (right), the shortest-path strategy can hardly capture the optimal DP evader. In comparison, though under a limited observation range of 2, the extended DP pursuers demonstrate significantly higher success rates. Besides, DP_{belief} consistently outperforms DP_{Pos}. This result verifies that the direct minimax policy (5) can be improved through belief averaging. Actually, since equation (5) treats all possible positions as equal, the result of the inner max can be very large when the size of Pos is large, leading to pessimistic pursuit behaviors like staying at certain "rest points."

We further take a look at how observation capabilities could affect success rates. We increase the observation range and evaluate the performance of DP_{belief} (6). As is shown in Table 6 (Appendix D.2), the success rates monotonically increase with the observation range and reach 100% when the range exceeds 5. While $D(\cdot)$ is an accurate estimator of the worst-case pursuit distance in Markov PEGs, it becomes an optimistic one under partial observability. Nevertheless, the experimental results show that combining this optimistic estimator with belief information can maintain the strength of the DP-based pursuit strategies, even under very limited observation capabilities.

5.2 Evaluations of Generalized RL Pursuers

Now, we implement and evaluate our cross-graph reinforcement learning method aimed at R2PS (Section 4). We discretize the maps from the Dungeon environment (Chen et al., 2019) to construct a synthetic training set containing 150 graphs and further include 150 random urban locations from Google Maps to create a large training set with a total of 300 graphs, where the maximum node number is no more than 500. We apply the R2PS learning scheme to the synthetic training set and the large training set. Appendix C.4 provides the learning curves of the pursuer policies under partial observability. As is shown in Figure 4, using the extended DP pursuers as guidance ($\beta = 0.1$) helps to improve the training efficiency over pure reinforcement learning ($\beta = 0$) under either training set.

Policy-Space Response Oracles (PSRO) (Lanctot et al., 2017) is a general reinforcement learning method extended from the game-theoretic approach of double oracle (DO) (McMahan et al., 2003) for equilibrium finding. Here we compare the zero-shot performance of our generalized pursuer policy with a PSRO policy that is directly trained on the

Table 2: Success Rate Comparison across Different Graphs and Strategies

Evader Policy	Stay		DP_{sync}		DP_{async}		BR_{async}
Pursuer Policy	Ours	PSRO	Ours	PSRO	Ours	PSRO	Ours
Grid Map	**1.00**	**1.00**	**1.00**	0.94	**1.00**	0.88	1.00
Scotland-Yard Map	**1.00**	**1.00**	**1.00**	0.47	**0.76**	0.00	0.73
Downtown Map	**1.00**	0.99	**1.00**	0.88	**0.99**	0.03	0.92
Times Square	**1.00**	0.93	**1.00**	0.16	**0.95**	0.04	0.27
Hollywood Walk of Fame	**1.00**	0.95	**0.90**	0.00	**0.38**	0.00	0.10
Sagrada Familia	**0.99**	0.93	**0.96**	0.07	**0.20**	0.00	0.20
The Bund	**1.00**	0.95	**0.92**	0.31	**0.25**	0.04	0.23
Eiffel Tower	**1.00**	0.99	**1.00**	0.97	**1.00**	0.52	0.55
Big Ben	**1.00**	0.99	**1.00**	0.29	**0.82**	0.24	0.65
Sydney Opera House	**1.00**	0.98	**1.00**	0.07	**0.95**	0.11	0.31

10 test graphs using 10 iterations (10000 episodes per iteration). Our RL policy aimed at R2PS, however, is pretrained under the synthetic training set with 150 graphs for 30000 episodes ($\beta = 0.1$) and then trained under the 150 random urban graphs for 70000 episodes. Since our training process never comes across the test graphs, our RL policy has to zero-shot generalize to these unseen graph structures during evaluations.

As is shown in Table 2, our pursuer policy consistently outperforms the PSRO pursuer policy in the real-world graphs against a variety of opponents, where:

- Stay corresponds to an evader that stays at the initial position. Since the initial distance between the pursuers and the evader is larger than the observation range, and the pursuers have no prior knowledge about the evader's policy, staying still is a reasonable strategy and leads to the occasional failure of these RL pursuers.

- DP_{sync} corresponds to the DP evader policy (2) under synchronous moves, and DP_{async} corresponds to the strictly optimal policy (3) under asynchronous moves. It is clear that the asynchronous-move evaders are much stronger than the synchronous-move ones due to the advantage of forecasting the pursuers' decisions. Against DP_{async}, the PSRO pursuers struggle under most of the test graphs in comparison with ours.

- BR_{async} corresponds to the best-responding asynchronous-move evader directly trained against our RL pursuers in the test graphs for 30000 episodes (converged). Even under this worst case, the success rates of our generalized pursuers are over 50% in half of the graphs.

Since our worst-case zero-shot performance is clearly better than the PSRO policy directly trained on the test graphs, we can say that our real-time strategies are worst-case robust even under varying graph structures, which implies that our approach achieves R2PS under partial observability.

5.3 Scalability Tests and Ablation Studies

Now we further verify the real-time pursuit capability under the graphs with higher complexity. We create another set of test graphs based on the seven famous locations in Table 1 (from Times Square to Sydney Opera House). Compared to the original graphs, the new graphs double both the map range and the discretization accuracy, leading to significantly larger node numbers. The success rates of our RL pursuer policy against the optimal evader DP_{async} and the inference time comparisons under an NVIDIA GeForce RTX 2080 Ti GPU are shown in Table 3. Clearly, our RL policy requires significantly smaller inference time in comparison with DP and maintains desirable overall performance under large graphs in comparison with the results in Table 2. Figure 6 (Appendix D.2) provides the scaling plots of our GNN-based RL policy inference and DP computation time.

We are also curious about whether our RL policy trained under the limited observation range of 2 can demonstrate better performance when the observation range is larger during inference time. As is shown in Table 7 (Appendix D.2), the success rates of our RL pursuers monotonically increase with the observation range. This additional result implies that our RL policy trained with the minimum observability can be directly applied to the cases with better sensing capabilities.

Table 3: RL Success Rate (against DP_{async}) and Comparison of Inference Time in Large Graphs

	Node Number	Sucess Rate	RL Time (s)	DP Time (s)
Times Square	1805	0.56	0.009837	101
Hollywood Walk of Fame	1251	0.46	0.007917	33
Sagrada Familia	2065	0.33	0.009895	139
The Bund	1723	0.46	0.008117	83
Eiffel Tower	1825	0.41	0.009616	96
Big Ben	1681	0.49	0.007752	79
Sydney Opera House	744	0.76	0.007648	6

Finally, we examine how the belief updates affect pursuit performance. As we have mentioned, our belief preservation (7) always employs a uniform evader policy ν since we could not access prior information about the true opponent. However, if we manage to obtain such information in reality, we can instantly improve the pursuit performance by replacing ν with the actual evader policy. As is shown in Table 4, utilizing known opponent information improves success rates against the best-responding evader BR_{async}. On the other hand, if we reduce the belief update frequency from every single step (original) to every 2 or 3 steps, then the pursuit success rates will instantly decline. This result further demonstrates the benefits of our belief update mechanism.

Table 4: RL Success Rate (against BR_{async}) Comparison under Different Belief Update Conditions

Belief Update Condition	Known Opponent	Original	Every 2 Steps	Every 3 Steps
Grid Map	1.00	1.00	0.60	0.42
Scotland-Yard Map	0.99	0.73	0.34	0.28
Downtown Map	1.00	0.92	0.61	0.39
Times Square	0.42	0.27	0.18	0.17
Hollywood Walk of Fame	0.13	0.10	0.04	0.03
Sagrada Familia	0.28	0.20	0.12	0.05
The Bund	0.54	0.23	0.13	0.12
Eiffel Tower	0.81	0.55	0.32	0.29
Big Ben	0.82	0.65	0.40	0.25
Sydney Opera House	0.54	0.31	0.22	0.15

6   Conclusion

This paper presents a novel approach to worst-case robust real-time pursuit strategies under partial observability and varying graph structures. We first theoretically examine a dynamic programming (DP) algorithm and prove that it can unify the solutions to Markov PEGs with either synchronous moves or asynchronous moves. Then, we propose a belief preservation mechanism to efficiently abstract evader information from the observation histories of the pursuers under partial observability. The belief information is combined with the distance table computed by the DP algorithm to derive observation-based pursuer policies, which demonstrates strong empirical performance against the perfect-information DP evader. Finally, we embed the belief preservation mechanism into the framework of EPG (Lu et al., 2025a) to find robust real-time pursuit strategies, fulfilling cross-graph reinforcement learning against the asynchronous-move DP evader under partial observability. Experiments show that our observation-based DP pursuers can be used as guidance to facilitate efficient policy exploration during RL training. Under unseen real-world graph structures, our cross-graph policy manages to generate real-time pursuit strategies with worst-case robustness, consistently outperforming the PSRO policy directly trained under the test graphs. Comparative results also reveal that the pursuers can benefit from belief updates, while the evader benefits from asynchronous moves.

In this work, the belief preservation mechanism provides an efficient way to handle partial observability. We show

that this mechanism can be effectively combined with the existing PEG methods like DP and EPG. After adversarial reinforcement learning across graphs, a generalized pursuer policy under belief preservation is eventually derived, leading to the first worst-case robust real-time pursuit strategies under partial observability. Hopefully, the current research on PEGs could encourage subsequent works on the broader research topics concerning real-world security.

References

Yuhong Cao, Tianxiang Hou, Yizhuo Wang, Xian Yi, and Guillaume Sartoretti. Ariadne: A reinforcement learning approach using attention-based deep networks for exploration. In *2023 IEEE International Conference on Robotics and Automation (ICRA)*, pp. 10219–10225. IEEE, 2023.

Fanfei Chen, Shi Bai, Tixiao Shan, and Brendan Englot. Self-learning exploration and mapping for mobile robots via deep reinforcement learning. In *Aiaa scitech 2019 forum*, pp. 0396, 2019.

Petros Christodoulou. Soft actor-critic for discrete action settings. *arXiv preprint arXiv:1910.07207*, 2019.

Tianzhe Chu, Yuexiang Zhai, Jihan Yang, Shengbang Tong, Saining Xie, Dale Schuurmans, Quoc V Le, Sergey Levine, and Yi Ma. SFT memorizes, RL generalizes: A comparative study of foundation model post-training. In *Forty-second International Conference on Machine Learning*, 2025.

Timothy H Chung, Geoffrey A Hollinger, and Volkan Isler. Search and pursuit-evasion in mobile robotics: A survey. *Autonomous robots*, 31:299–316, 2011.

Wojciech M Czarnecki, Gauthier Gidel, Brendan Tracey, Karl Tuyls, Shayegan Omidshafiei, David Balduzzi, and Max Jaderberg. Real world games look like spinning tops. *Advances in Neural Information Processing Systems*, 33: 17443–17454, 2020.

M Fromme and M Aigner. A game of cops and robbers. *Discrete Appl. Math*, 8:1–12, 1984.

Arthur S Goldstein and Edward M Reingold. The complexity of pursuit on a graph. *Theoretical computer science*, 143 (1):93–112, 1995.

Tuomas Haarnoja, Aurick Zhou, Kristian Hartikainen, George Tucker, Sehoon Ha, Jie Tan, Vikash Kumar, Henry Zhu, Abhishek Gupta, Pieter Abbeel, et al. Soft actor-critic algorithms and applications. *arXiv preprint arXiv:1812.05905*, 2018.

Hado Hasselt. Double Q-learning. *Advances in Neural Information Processing Systems*, 23, 2010.

Karel Horák and Branislav Bošanský. Dynamic programming for one-sided partially observable pursuit-evasion games. In *International Conference on Agents and Artificial Intelligence*, volume 2, pp. 503–510. SCITEPRESS, 2017.

Marc Lanctot, Vinicius Zambaldi, Audrunas Gruslys, Angeliki Lazaridou, Karl Tuyls, Julien Pérolat, David Silver, and Thore Graepel. A unified game-theoretic approach to multiagent reinforcement learning. *Advances in Neural Information Processing Systems*, 30, 2017.

Pengdeng Li, Shuxin Li, Xinrun Wang, Jakub Cerný, Youzhi Zhang, Stephen McAleer, Hau Chan, and Bo An. Grasper: A generalist pursuer for pursuit-evasion problems. In *Proceedings of the 23rd International Conference on Autonomous Agents and Multiagent Systems*, pp. 1147–1155, 2024.

Shuxin Li, Xinrun Wang, Youzhi Zhang, Wanqi Xue, Jakub Černý, and Bo An. Solving large-scale pursuit-evasion games using pre-trained strategies. In *Proceedings of the AAAI Conference on Artificial Intelligence*, volume 37, pp. 11586–11594, 2023.

Runyu Lu, Peng Zhang, Ruochuan Shi, Yuanheng Zhu, Dongbin Zhao, Yang Liu, Dong Wang, and Cesare Alippi. Equilibrium policy generalization: A reinforcement learning framework for cross-graph zero-shot generalization in pursuit-evasion games. In *The Thirty-ninth Annual Conference on Neural Information Processing Systems*, 2025a.

Runyu Lu, Yuanheng Zhu, and Dongbin Zhao. Divergence-regularized discounted aggregation: Equilibrium finding in multiplayer partially observable stochastic games. In *The Thirteenth International Conference on Learning Representations*, 2025b.

Kostas Margellos and John Lygeros. Hamilton-Jacobi formulation for reach-avoid differential games. *IEEE Transactions on Automatic Control*, 56(8):1849–1861, 2011.

H Brendan McMahan, Geoffrey J Gordon, and Avrim Blum. Planning in the presence of cost functions controlled by an adversary. In *Proceedings of the 20th International Conference on Machine Learning (ICML-03)*, pp. 536–543, 2003.

Christos H Papadimitriou and John N Tsitsiklis. The complexity of Markov decision processes. *Mathematics of operations research*, 12(3):441–450, 1987.

Tim Roughgarden. *Twenty lectures on algorithmic game theory*. Cambridge University Press, 2016.

Lloyd S Shapley. Stochastic games. *Proceedings of the National Academy of Sciences*, 39(10):1095–1100, 1953.

Ashish Vaswani, Noam Shazeer, Niki Parmar, Jakob Uszkoreit, Llion Jones, Aidan N Gomez, Łukasz Kaiser, and Illia Polosukhin. Attention is all you need. *Advances in Neural Information Processing Systems*, 30, 2017.

Rene Vidal, Shahid Rashid, Cory Sharp, Omid Shakernia, Jin Kim, and Shankar Sastry. Pursuit-evasion games with unmanned ground and aerial vehicles. In *Proceedings 2001 ICRA. IEEE International Conference on Robotics and Automation (Cat. No. 01CH37164)*, volume 3, pp. 2948–2955. IEEE, 2001.

Rene Vidal, Omid Shakernia, H Jin Kim, David Hyunchul Shim, and Shankar Sastry. Probabilistic pursuit-evasion games: Theory, implementation, and experimental evaluation. *IEEE Transactions on Robotics and Automation*, 18 (5):662–669, 2002.

Marcos AM Vieira, Ramesh Govindan, and Gaurav S Sukhatme. Optimal policy in discrete pursuit-evasion games. *Department of Computer Science, University of Southern California, Tech. Rep*, 2008.

Oriol Vinyals, Meire Fortunato, and Navdeep Jaitly. Pointer networks. *Advances in Neural Information Processing Systems*, 28, 2015.

Zonghan Wu, Shirui Pan, Fengwen Chen, Guodong Long, Chengqi Zhang, and Philip S Yu. A comprehensive survey on graph neural networks. *IEEE Transactions on Neural Networks and Learning Systems*, 32(1):4–24, 2020.

Wanqi Xue, Youzhi Zhang, Shuxin Li, Xinrun Wang, Bo An, and Chai Kiat Yeo. Solving large-scale extensive-form network security games via neural fictitious self-play. In *Proceedings of the 28th International Joint Conference on Artificial Intelligence*, 2021.

Wanqi Xue, Bo An, and Chai Kiat Yeo. NSGZero: Efficiently learning non-exploitable policy in large-scale network security games with neural Monte Carlo tree search. In *Proceedings of the AAAI Conference on Artificial Intelligence*, volume 36, pp. 4646–4653, 2022.

Chao Yu, Akash Velu, Eugene Vinitsky, Jiaxuan Gao, Yu Wang, Alexandre Bayen, and Yi Wu. The surprising effectiveness of PPO in cooperative multi-agent games. *Advances in Neural Information Processing Systems*, 35: 24611–24624, 2022.

Zhengyuan Zhou, Ryo Takei, Haomiao Huang, and Claire J Tomlin. A general, open-loop formulation for reach-avoid games. In *2012 IEEE 51st IEEE Conference on Decision and Control (CDC)*, pp. 6501–6506. IEEE, 2012.

Shuxin Zhuang, Shuxin Li, Tianji Yang, Muheng Li, Xianjie Shi, Bo An, and Youzhi Zhang. Solving urban network security games: Learning platform, benchmark, and challenge for AI research. *arXiv preprint arXiv:2501.17559*, 2025.

A   Omitted Proofs

A.1   Proof of Theorem 1

Proof. For no-exit PEGs, the Nash value satisfies the following Bellman minimax equation:

$$
V^*(s) = \begin{cases} \max\limits_{\mu(s)\in\Delta(\mathcal{A})} \min\limits_{b\in\mathcal{B}} \sum\limits_{a\in\mathcal{A}} \mu(s,a)\left(r(s,a,b) + \gamma \sum\limits_{s'\in S} \mathcal{P}(s,a,b,s')V^*(s')\right) & f(s) = 0, \\ 1 & f(s) = 1. \end{cases}
$$

Since the transition is deterministic and a non-zero reward is received only when a termination state is reached, we can simplify the Bellman equation as follows:

$$
V^*(s) = \begin{cases} \max\limits_{\mu(s)\in\Delta(\mathcal{A})} \min\limits_{b\in\mathcal{B}} \sum\limits_{a\in\mathcal{A}} \mu(s,a)\gamma V^*(s' = \mathcal{P}(s,a,b)) & f(s) = 0, \\ 1 & f(s) = 1. \end{cases}
$$

The equilibrium policy for the max-player satisfies:

$$
\mu^*(s) \in \underset{\mu(s)\in\Delta(\mathcal{A})}{\arg\max} \left\{ \min_{b\in\mathcal{B}} \sum_{a\in\mathcal{A}} \mu(s,a)V^*(s' = \mathcal{P}(s,a,b)) \right\}.
$$

When there is a pure-strategy Nash equilibrium in the game, the $\arg\max$ has a pure-strategy solution, and the Bellman equation can be further simplified:

$$
V^*(s) = \gamma \max_{a\in\mathcal{A}} \min_{b\in\mathcal{B}} V^*(s' = \mathcal{P}(s,a,b)). \tag{9}
$$

Note that the Nash value has the form of $V^*(s) = \gamma^d (d \in \mathbb{N})$. Therefore, we consider using mathematical induction. We assume that $V^*(s) = \gamma^{D(s)}$ holds for all states s that satisfies either $V^*(s) = \gamma^d$ or $D(s) = d$ when $d < k$ $(\gamma^d > \gamma^k)$. We want to prove that $V^*(s) = \gamma^{D(s)}$ holds for all states s that satisfies either $V^*(s) = \gamma^k$ or $D(s) = k$. Clearly, our initialization guarantees that the proposition holds for $k = 0$. Our update condition $D(n_p, n_e) = \infty$ guarantees that every state $s \in S$ is pushed into and popped from $\mathcal{Q}$ at most once. Note that the following proof reverses the notations of s and s' in (9) to better align with $s = (s_p, s_e)$ in Algorithm 1.

Now, we prove the first half of the proposition. For an arbitrary state $s' = (n_p, n_e)$ that satisfies $V^*(s') = \gamma^k$, the simplified Bellman equation (9) guarantees that there exists $a = s_p \in \mathcal{A}(n_p)$ and $b = s_e \in \mathcal{B}(n_e)$ such that $V^*(s') = \gamma V^*(s = \mathcal{P}(s',a,b))$. Therefore, there exists $s = (s_p, s_e)$ such that $V^*(s) = \gamma^{k-1}$. According to the first half of the induction hypothesis, we have that $D(s) = k - 1 < \infty$, which implies that the algorithm once pushed s' into $\mathcal{Q}$. Besides, the Bellman equation guarantees that $\forall b' \in \mathcal{B}(n_e), V^*(\mathcal{P}(s',a,b')) \geq V^*(\mathcal{P}(s',a,b)) = V^*(s) = \gamma^{k-1} > \gamma^k$. By induction hypothesis, $D(s_p, n_e') \leq D(s_p, s_e)$ holds for any neighbor n_e' of n_e. Therefore, the algorithm must enumerate n_e when popping $s = (s_p, s_e)$. If we have $D(n_p, n_e) = \infty$ at the moment, then n_p will be enumerated in the inner loop, and we will have $D(n_p, n_e) = D(s_p, s_e) + 1 = k$. Now we complete the proof by showing that $D(n_p, n_e) < \infty$ implies $D(n_p, n_e) = k$. Actually, if $k < D(n_p, n_e) < \infty$, then $D(s')$ must be computed by adding 1 to some $D(s'') \geq k$. Since s'' must be popped from $\mathcal{Q}$ no later than s, it is contradictory to the fact that $D(s'') > D(s) = k - 1$. If $D(n_p, n_e) < k$, then the second half of the induction hypothesis implies that $V^*(s') = \gamma^{D(n_p, n_e)}$, which is contradictory to the fact that $V^*(s') = \gamma^k$.

Then, we prove the second half of the proposition. For an arbitrary state $s' = (n_p, n_e)$ that satisfies $D(s') = k$, the $D(s)$ must be computed by adding 1 to some $D(s) = k - 1$, where $s = (s_p, s_e)$. According to the first half of the induction hypothesis, we have $V^*(s) = \gamma^k$. The algorithm guarantees that $D(s_p, n_e') \leq D(s_p, s_e) = k - 1$ holds for any neighbor n_e' of n_e. By induction hypothesis, it holds that $\forall b' \in \mathcal{B}(n_e), V^*(\mathcal{P}(s',a,b')) \geq V^*(\mathcal{P}(s',a,b))$ when $a = s_p \in \mathcal{A}(n_p)$ and $b = s_e \in \mathcal{B}(n_e)$. Therefore, $\min\limits_{b\in\mathcal{B}(n_e)} V^*(\mathcal{P}(s',a,b)) = \gamma^{k-1}$ when $a = s_p \in \mathcal{A}(n_p)$. If there exists $a^\dagger = s_p^\dagger \in \mathcal{A}(n_p)$ such that $\min\limits_{b\in\mathcal{B}(n_e)} V^*(\mathcal{P}(s',a',b)) > \gamma^{k-1}$, then we let $b^\dagger = \arg\min\limits_{b\in\mathcal{B}(n_e)} V^*(\mathcal{P}(s',a^\dagger,b)) > \gamma^{k-1}$ and let $s^\dagger = (s_p^\dagger, s_e^\dagger = b^\dagger)$. According to the first half of the induction hypothesis, $D(s_p^\dagger, n_e') \leq D(s_p^\dagger, s_e^\dagger) < k - 1$ holds for any neighbor n_e' of n_e. Since $D(s_p^\dagger, s_e^\dagger) < D(s_p, s_e)$, $s^\dagger$ must be popped from $\mathcal{Q}$ earlier than s, which means that $D(s) = \infty$ when $s^\dagger$ is popped. Therefore, $s' = (n_p, n_e)$ must be enumerated when $s^\dagger$ is popped, which is contradictory to the fact that $D(s') = \infty$ when s is popped. Therefore, $V^*(s') = \gamma \max\limits_{a\in\mathcal{A}} \min\limits_{b\in\mathcal{B}} V^*(\mathcal{P}(s',a,b)) = \gamma^k$.

13

For now, we have proved that $V^*(s) = \gamma^{D(s)}$. Therefore:

$$\mu^*(s_p, s_e) = \underset{\text{neighbor } n_p \text{ of } s_p}{\arg \min} \left\{ \underset{\text{neighbor } n_e \text{ of } s_e}{\max} D(n_p, n_e) \right\} \Rightarrow \mu^*(s) = \underset{a \in \mathcal{A}}{\arg \max} \underset{b \in \mathcal{B}}{\min} V^*(\mathcal{P}(s, a, b)),$$

$$\nu^*(s_p, s_e) = \underset{\text{neighbor } n_e \text{ of } s_e}{\arg \max} \left\{ \underset{\text{neighbor } n_p \text{ of } s_p}{\min} D(n_p, n_e) \right\} \Rightarrow \nu^*(s) = \underset{b \in \mathcal{B}}{\arg \min} \underset{a \in \mathcal{A}}{\max} V^*(\mathcal{P}(s, a, b)).$$

As there exists a pure-strategy Nash equilibrium, it is directly guaranteed that (μ^*, ν^*) is a Nash equilibrium. $\qquad \square$

A.2 Proof of Lemma 1

Proof. We consider the cases of $D(n_p, n_e) = \infty$ and $0 < D(n_p, n_e) < \infty$, separately.

The first case is $D(n_p, n_e) = \infty$, which implies that (n_p, n_e) is never enqueued:

Suppose that $\min\limits_{\text{neighbor } s_p \text{ of } n_p} \left\{ \max\limits_{\text{neighbor } s_e \text{ of } n_e} D(s_p, s_e) \right\} < \infty$. Then, we let

$$s_p = \underset{\text{neighbor } s_p \text{ of } n_p}{\arg\min} \left\{ \max\limits_{\text{neighbor } s_e \text{ of } n_e} D(s_p, s_e) \right\}, s_e = \underset{\text{neighbor } s_e \text{ of } n_e}{\arg\max} D(s_p, s_e).$$

Since $D(s_p, s_e) = \min\limits_{\text{neighbor } s_p \text{ of } n_p} \left\{ \max\limits_{\text{neighbor } s_e \text{ of } n_e} D(s_p, s_e) \right\} < \infty$, (s_p, s_e) is once enqueued.

Since $s_e = \underset{\text{neighbor } s_e \text{ of } n_e}{\arg\max} D(s_p, s_e)$, we have that $\nexists n_e' \in \mathcal{V}, (n_e, n_e') \in E, D(s_p, n_e') > D(s_p, s_e)$. Since $D(n_p, n_e) = \infty$, state (n_p, n_e) will be enumerated when (s_p, s_e) is dequeued. Then, $D(n_p, n_e)$ is enqueued, which leads to a contradiction.

Therefore, we have $\min\limits_{\text{neighbor } s_p \text{ of } n_p} \left\{ \max\limits_{\text{neighbor } s_e \text{ of } n_e} D(s_p, s_e) \right\} = \infty$, which means the equation holds in the first case.

The second case is $0 < D(n_p, n_e) < \infty$, which implies that (n_p, n_e) is once enumerated when a state $(s_p, s_e) \in$ Neighbor(n_p, n_e) is dequeued. According to the enumeration rule, we have $\nexists n_e' \in \mathcal{V}, (n_e, n_e') \in E, D(s_p, n_e') > D(s_p, s_e)$, which implies $s_e = \underset{\text{neighbor } s_e \text{ of } n_e}{\arg\max} D(s_p, s_e)$. Since $D(n_p, n_e) = D(s_p, s_e) + 1$, we have:

$$D(n_p, n_e) \geq \min\limits_{\text{neighbor } s_p \text{ of } n_p} \left\{ \max\limits_{\text{neighbor } s_e \text{ of } n_e} D(s_p, s_e) \right\} + 1.$$

Now redefine $s_p = \underset{\text{neighbor } s_p \text{ of } n_p}{\arg\min} \left\{ \max\limits_{\text{neighbor } s_e \text{ of } n_e} D(s_p, s_e) \right\}, s_e = \underset{\text{neighbor } s_e \text{ of } n_e}{\arg\max} D(s_p, s_e).$

Then, we have $D(s_p, s_e) = \min\limits_{\text{neighbor } s_p \text{ of } n_p} \left\{ \max\limits_{\text{neighbor } s_e \text{ of } n_e} D(s_p, s_e) \right\}$ and $\nexists n_e' \in \mathcal{V}, (n_e, n_e') \in E, D(s_p, n_e') > D(s_p, s_e)$. Since the D values in $\mathcal{Q}$ do not decrease, we have:

$$D(n_p, n_e) \leq D(s_p, s_e) + 1 = \min\limits_{\text{neighbor } s_p \text{ of } n_p} \left\{ \max\limits_{\text{neighbor } s_e \text{ of } n_e} D(s_p, s_e) \right\} + 1.$$

Therefore, $D(n_p, n_e) = \min\limits_{\text{neighbor } s_p \text{ of } n_p} \left\{ \max\limits_{\text{neighbor } s_e \text{ of } n_e} D(s_p, s_e) \right\} + 1$ holds in the second case.

To conclude, the equation always holds when $D(n_p, n_e) > 0$. $\qquad\square$

A.3 Proof of Theorem 2

Proof. First, we prove that for any state $s = (s_p, s_e)$ satisfying $D(s) = d < \infty$, μ^* guarantees pursuit within d steps against any evasion strategy:

Clearly, the proposition holds true when $d = 0$. Assume that the proposition holds for all $d < k$. When $d = k$, we let $n_p = \underset{\text{neighbor } n_p \text{ of } s_p}{\arg\min} \left\{ \underset{\text{neighbor } n_e \text{ of } s_e}{\max} D(n_p, n_e) \right\}, n_e = \underset{\text{neighbor } n_e \text{ of } s_e}{\arg\max} D(n_p, n_e)$. By Lemma 1, we have $D(n_p, n_e') \leq D(n_p, n_e) = D(s_p, s_e) - 1 \leq k - 1 < k, \forall n_e' \in \text{Neighbor}(s_e)$. By induction hypothesis, μ^* guarantees pursuit within $k - 1$ steps for the states (n_p, n_e') that satisfies $n_e' \in \text{Neighbor}(s_e)$. Therefore, $\mu^*(s) = n_p$ guarantees pursuit within k steps. By induction, the proposition holds true for all $d < \infty$.

Second, we prove that for any state $s = (s_p, s_e)$ satisfying $D(s) = d < \infty$, ν^* avoids being captured in less than d steps by any pursuit strategy:

Suppose there exists a pursuit movement sequence $\{n_p^0, n_p^1, \cdots, n_p^{T-1}\}$ that captures the evader within $T < d$ steps under policy ν^*. Then, we denote by $\{s^0, s^1, s^2, \cdots, s^T\}$ the corresponding state sequence, where $s_0 = s$ and $D(s^T) = 0$. By Lemma 1, $D(s_p, s_e) = \underset{\text{neighbor } n_p \text{ of } s_p}{\min} \{\nu^*(s_p, s_e, n_p)\} + 1$, which implies that $D(s_p, s_e) \geq D(n_p, \nu^*(s_p, s_e, n_p)) + 1, \forall n_p$. Therefore, $D(s^t) = D(s_p^t, s_e^t) \geq D(n_p^t, \nu^*(s_p^t, s_e^t, n_p^t)) + 1 = D(s_p^{t+1}, s_e^{t+1}) + 1 = D(s^{t+1}) + 1$. This leads to a contradiction: $D(s) = D(s^0) \geq D(s^1) + 1 \geq D(s^2) + 2 \geq D(s^T) + T = T < d = D(s)$. Therefore, ν^* always avoids being captured in less than d steps when $D(s) = d < \infty$. □

A.4 Proof of Corollary 1

Proof. By Theorem 2:

For $s = (s_p, s_e)$ with $D(s) = d < \infty$, since μ^* guarantees pursuit within d steps against any evasion strategy, no evader can guarantee evasion for d steps against a worst-case pursuit strategy. Since ν^* avoids being captured in less than d steps by any pursuit strategy, ν^* is the optimal evasion strategy.

For $s = (s_p, s_e)$ with $D(s) = d < \infty$, since ν^* avoids being captured in less than d steps by any pursuit strategy, no pursuer can guarantee pursuit in less than d steps against a worst-case evasion strategy. Since μ^* guarantees pursuit within d steps against any evasion strategy, μ^* is the optimal pursuit strategy. □

A.5 Proof of Theorem 3

Proof. Suppose that there exists a pursuit strategy that captures ν^* within T steps.

In this case, we denote by $\{s^0, s^1, s^2, \cdots, s^T\}$ the state sequence of a successful pursuit, where $s_0 = s$ and $D(s^T) = 0$. By Lemma 1, $D(s_p, s_e) = \underset{\text{neighbor } n_p \text{ of } s_p}{\min} \{D(n_p, \nu^*(n_p))\} + 1$, which implies $D(n_p, \nu^*(n_p)) = \infty, \forall n_p \in \text{Neighbor}(s_p)$. Then, we have $D(s^0) = \infty \Rightarrow D(s^1) = \infty \Rightarrow \cdots \Rightarrow D(s^T) = \infty$, which leads to a contradiction.

Therefore, for $s = (s_p, s_e)$ with $D(s) = \infty$, ν^* can never be captured by any pursuit strategy. □

A.6 Proof of Lemma 2

Proof. When Pos is a singleton, we have $\text{Pos} = \{s_e\}$. Therefore,

$$\mu(s_p, \text{Pos}) = \underset{\text{neighbor } n_p \text{ of } s_p}{\arg\min} \left\{ \max_{n_e \in \text{Neighbor(Pos)}} D(n_p, n_e) \right\}$$

$$= \underset{\text{neighbor } n_p \text{ of } s_p}{\arg\min} \left\{ \max_{\text{neighbor } n_e \text{ of } s_e} D(n_p, n_e) \right\} = \mu^*(s_p, s_e).$$

Besides, we have

$$\text{belief(s)} = \begin{cases} 0 & s \notin \text{Pos} \\ \displaystyle\sum_{\text{neighbor } v \text{ of } s} \nu(v, s) \text{belief}_{\text{old}}(v) & s \in \text{Pos} \end{cases}$$

$$= \mathbb{I}[s = s_e] \, \text{belief}_{\text{new}}(s_e).$$

Therefore, it holds that

$$\mu(s_p, \text{belief}) = \underset{\text{neighbor } n_p \text{ of } s_p}{\arg\min} \left\{ \frac{\text{belief}_{\text{new}}(s_e) \max_{\text{neighbor } n_e \text{ of } s_e} D(n_p, n_e)}{\text{belief}_{\text{new}}(s_e)} \right\}$$

$$= \underset{\text{neighbor } n_p \text{ of } s_p}{\arg\min} \left\{ \max_{\text{neighbor } n_e \text{ of } s_e} D(n_p, n_e) \right\} = \mu^*(s_p, s_e).$$

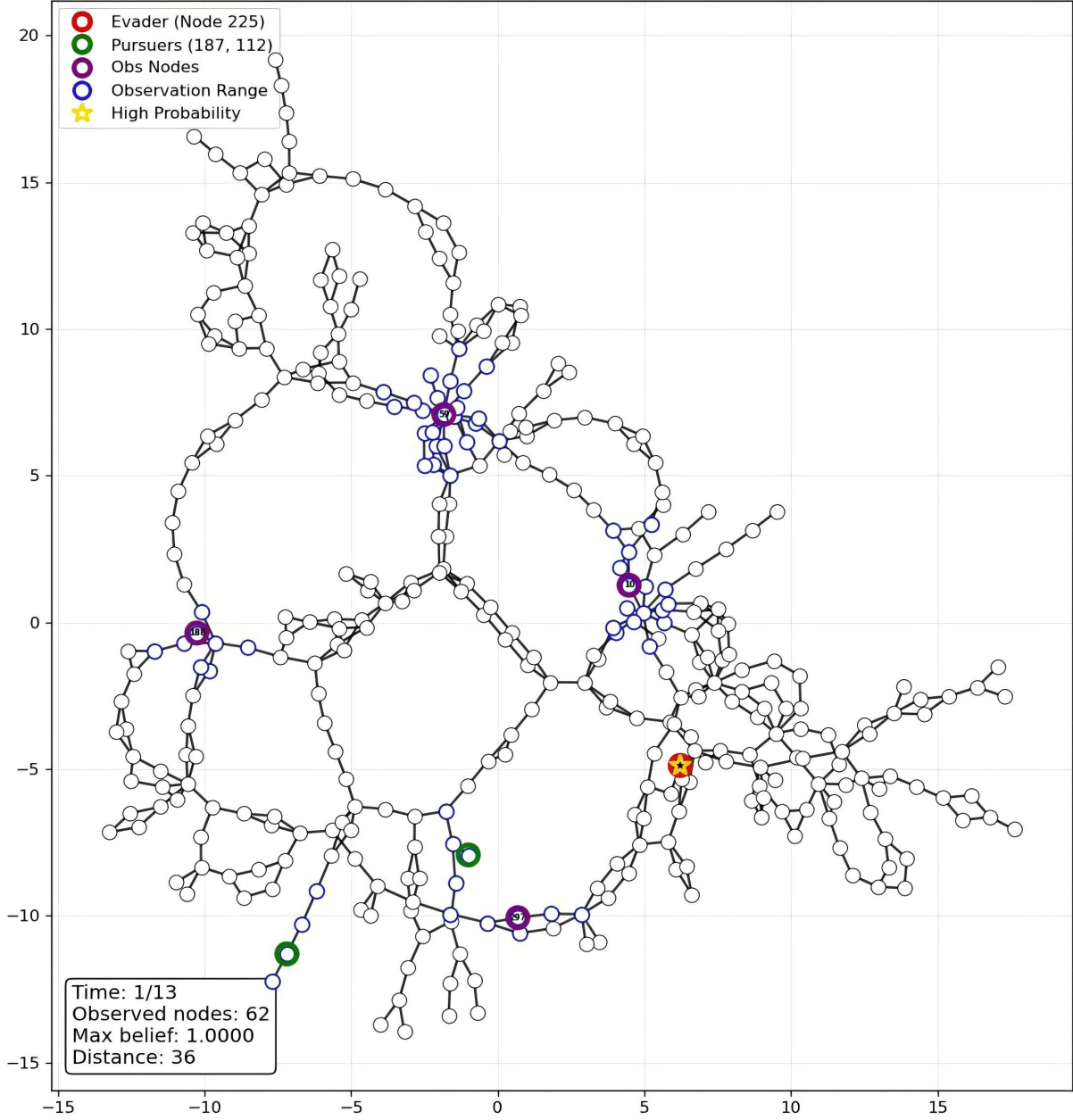$\square$

B Illustration of Belief Preservation

Figure 2: Pursuit Initialization under Limited Observation Range (Nodes with Blue Outlines)

Figure 2 illustrates the initial state of one pursuit episode. Two green pursuers with an observation range of 2 are going to capture the red evader that stays still within a total of 13 steps. The purple nodes are some auxiliary sensors that provide additional information for the pursuers (also with an observation range of 2). Therefore, all of the nodes with dark blue outlines can be observed by the pursuers, while the other nodes cannot. At the first step, only the red node has non-zero belief and is marked as high probability (represented by the yellow star).

Figure 3 illustrates the pursuit process under belief preservation, where the black or shadowed area around the evader corresponds to belief and the darkness of the nodes indicates the current belief distribution. Following (7), the belief is spread as the game proceeds (see timesteps $2, 4, 6, 8, 10$) and used to generate the pursuit strategy (6) under partial observability. At timestep 12, the evader is eventually observed. Since Pos becomes a singleton by (4), the
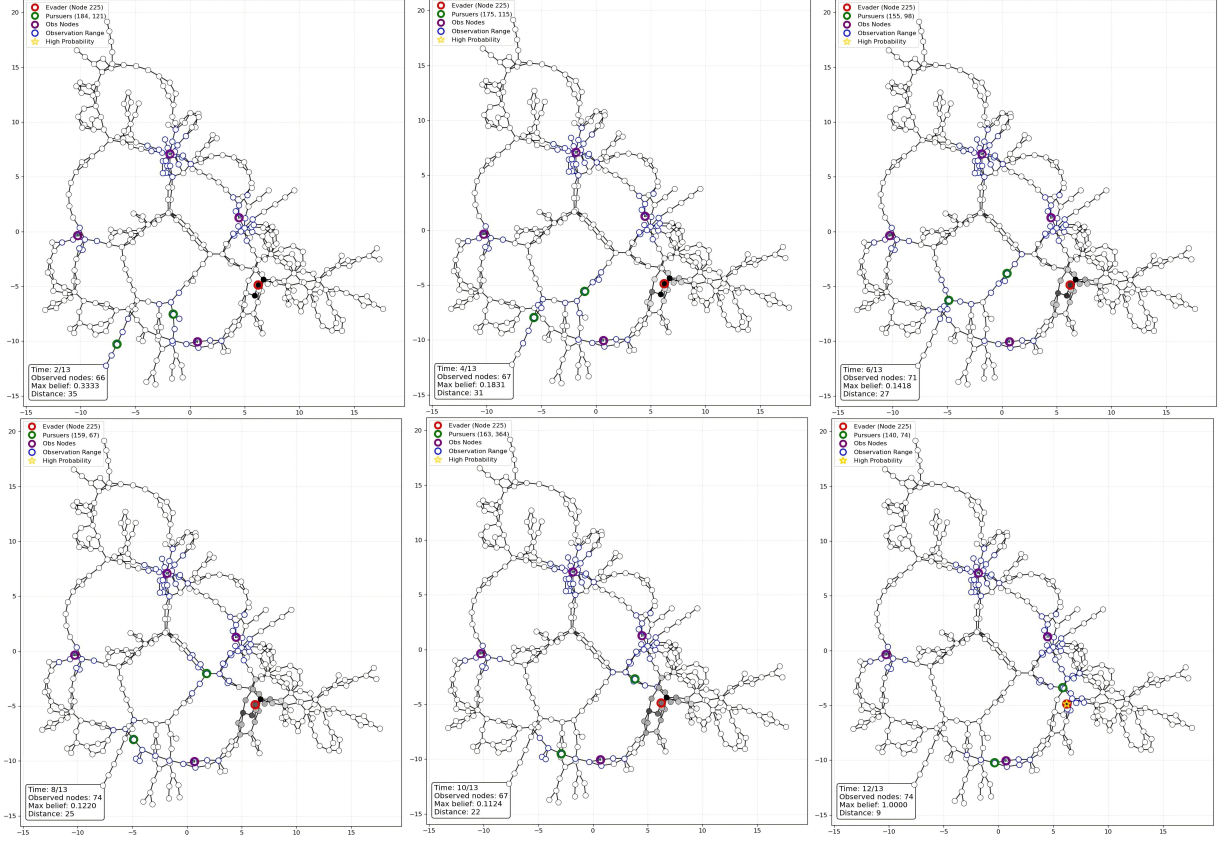
Figure 3: Pursuit Illustration under Belief Preservation (Shadowed Area around Evader)

shadowed area disappears, and the observed evader node is marked as high probability again.

Note that when the observed area covers all nodes, the game will be reduced to its perfect-information counterpart, where the DP pursuer policy is provably optimal.

C   Implementation Details

C.1   Soft Actor-Critic (SAC)

To fulfill R2PS training, we use discrete-action soft-actor critic (SAC) (Christodoulou, 2019) as the backbone RL algorithm, where:

The value function is defined as

$$V(s) = \mathbb{E}_{a \sim \pi(s)} \left[Q(s, a) - \alpha \log \pi(s, a) \right].$$

The loss of the value network Q_ϕ is computed as

$$J_Q(\phi) = \mathbb{E}_{s,a} \left[\frac{1}{2} (Q_\phi(s, a) - (r + \gamma \mathbb{E}_{s'} \left[V(s') \right]))^2 \right].$$

The loss of the policy network π_θ is computed as

$$J_\pi(\theta) = \mathbb{E}_{s,a \sim \pi_\theta(s)} \left[\alpha \log \pi_\theta(s, a) - Q(s, a) \right].$$

The temperature α under target entropy $\overline{H}$ is adaptively updated under loss

$$J(\alpha) = \mathbb{E}_{s,a} \left[-\alpha \left(\log \pi(s, a) + \overline{H} \right) \right].$$

C.2   Graph Neural Network (GNN)

We employ a sequence model with a parameter-sharing graph neural network (GNN) architecture (Lu et al., 2025a) to represent the graph-based policy of the homogeneous pursuers:

Under the principle of sequential decision-making, a joint policy can be decomposed as

$$\pi(a_1, a_2, \cdots, a_m | s) = \prod_{l=1}^{m} \pi(a_l | s, a_1, \cdots, a_{l-1}),$$

where $(s, a_1, \cdots, a_{l-1})$ indicates the global state after the first $l - 1$ pursuers take actions $(a_i)_{i \in [l-1]}$.

For a team of pursuers with m agents, the sequence model queries the policy network m times under a fixed adjacent matrix $M \in \{0, 1\}^{n \times n}$ ($n = |\mathcal{V}|$) for the current graph. The input is composed of a state feature s_f and the information of node index c for the current acting agent. Note that under partial observability, the global state s is replaced by $(s_p, \text{Pos}, \text{belief})$. We use the shortest path distances to the m pursuers as the initial feature of each node $v \in \mathcal{V}$. The normalized features of all n nodes are concatenated with $(\text{Pos}, \text{belief})$ to construct the state feature s_f. Also note that the distances between one node and all other nodes can be computed using the $\mathcal{O}(n^2)$ Dijkstra algorithm.

Given the state feature input s_f, we embed it into $\mathbb{R}^{d \times n}$ and send the result into an encoder composed of 6 self-attention layers, where d is the embedding dimension. Each layer takes the output h of the last layer as the input and outputs h' using a masked attention, whose time complexity is also $\mathcal{O}(n^2)$:

$$q_i = W_Q h_i, k_i = W_K h_i, \ v_i = W_V h_i, u_{ij} = \frac{q_i^T k_j}{\sqrt{d}}, w_{ij} = \frac{e^{u_{ij}}}{\sum_{t=1}^{n} e^{u_{it}}}, h_i' = \sum_{j=1}^{n} \min \{w_{ij}, M_{ij}\} v_j,$$

where $W_Q, W_K, W_V \in \mathbb{R}^{d \times d}$ are the weights to be learned.

Given the output of the encoder $\hat{h}$, we employ a decoder without masks to gather global information. The decoder uses $\hat{h}_c$ to query in the output features $\hat{h}$ of all nodes, with the keys equal to the values:

$$q = W_Q \hat{h}_c, k_i = W_K \hat{h}_i, v_i = W_V \hat{h}_i, u_j = \frac{q^T k_j}{\sqrt{d}}, w_j = \frac{e^{u_j}}{\sum_{t=1}^{n} e^{u_t}}, \tilde{h}_c = \sum_{j=1}^{n} w_j v_j.$$

The decoder output $\tilde{h}_c$ is further concatenated with $\hat{h}_c$ and projected into $\mathbb{R}^d$. Then, it is used as a query for a pointer network, which takes the features of the neighbor nodes $\hat{h}_{ne}$ for the current agent as the keys and values. The pointer network directly outputs the attention vector w as the current policy $\pi(\cdot|s)$ since the number of the neighbors aligns with the number of the valid actions. After the first query through the policy network, an action a_1 for the first agent is sampled from $\pi(\cdot|s)$, and the state is updated as $s' = (s, a_1)$. The subsequent $m - 1$ queries follow the same process as above.

C.3   Hyperparameter Setting

Table 5 shows the detailed hyperparameter setting used in the training of our RL pursuer policy.

Table 5: Hyperparameter Setting of R2PS Training

Discount factor γ	0.99
SAC target entropy coefficient	0.05
GNN embedding dimension d	128
GNN attention heads	8
Batch size	128
Learning rate	10^{-5}
Update epoch	8

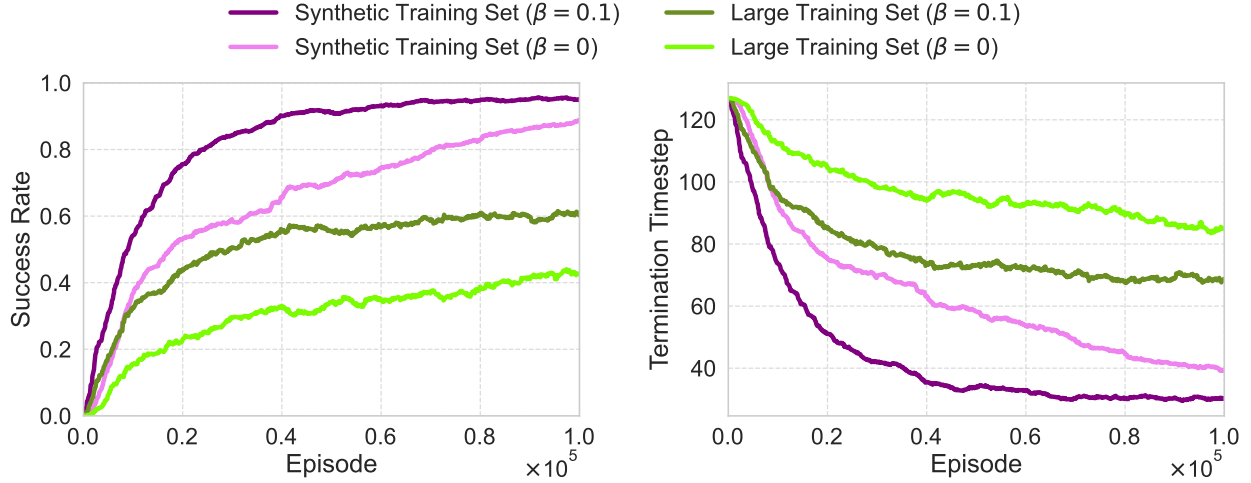## C.4   Learning Curves of RL Pursuers

Figure 4: Cross-Graph Learning Curves of Generalized Pursuer Policies

During the cross-graph R2PS training, we consider the use of $\beta = 0.1$ and $\beta = 0$ in the policy loss $\mathcal{L}(\theta)$ (8). For the former, we employ the belief-averaged DP policy (6) as the reference policy. For the latter, it means that the training process is without policy guidance. Figure 4 shows the learning curves of our RL pursuer policies. Clearly, training with policy guidance is more efficient than pure reinforcement learning under SAC loss. This comparison verifies that the DP pursuer policy can serve as guidance to facilitate efficient exploration of the cross-graph RL policy. Besides, training under the synthetic training set is relatively easier than under the large one that contains more real-world graph structures. Nevertheless, our R2PS learning scheme gradually improves the quality of the RL pursuer policies under all of the four settings, using a very limited observation range of 2.

21

D Experimental Details
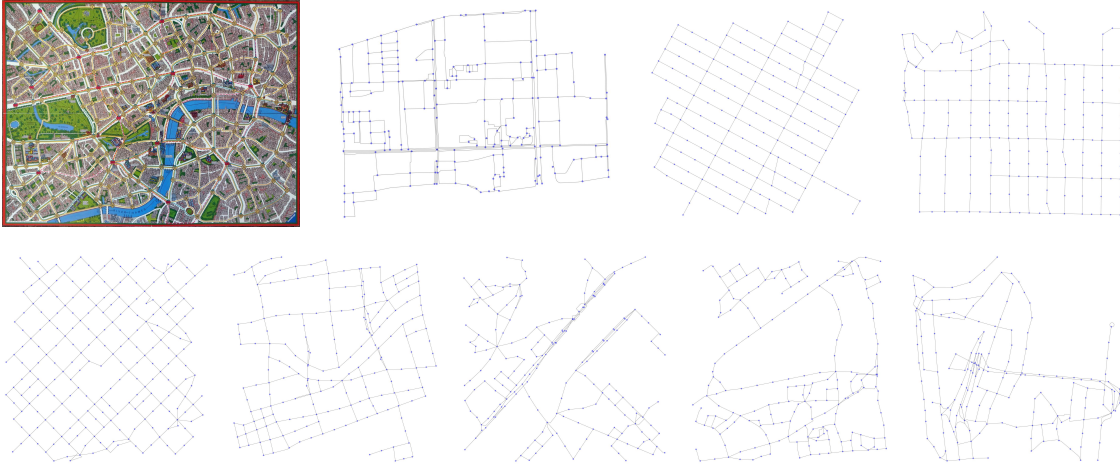
D.1 Details of Test Graphs

Figure 5: Illustration of Test Graphs (Starting from Scotland-Yard Map)

The test graphs for both DP and RL pursuers include Grid Map (a 10×10 grid), Scotland-Yard Map (from the board game Scotland-Yard), Downtown Map (a real-world location from Google Maps), and 7 famous real-world spots (from Times Square to Sydney Opera House). The graph structures are illustrated in Figure 5, following the order in Table 1.

The real-world graphs are generated through a program designed for discretizing the regions around the location centers in Google Maps. The map range is set to be 600 by default (corresponding to a radius of 600 meters). Nodes correspond to actual road intersections, endpoints, and geometry-defined shape points along roadways. Edges represent the physical road segments connecting these nodes, typically encoded as polylines that capture the true geometry of each street. To ensure a topologically coherent intersection structure, closely spaced intersection points (within 20 meters of one another) are abstracted into single representative nodes. After establishing the intersection-level skeleton, the program further adjusts the spatial resolution by subdividing any road segment whose length exceeds 100 (discretization granularity) meters. For such long segments, the program inserts additional intermediate points at regular intervals along the original road geometry. These newly added points are treated as supplementary nodes, and the original long segment is replaced by several shorter segments. The resulting graph therefore adopts a hybrid granularity: true intersections are preserved as primary nodes, while long road segments are discretized into shorter units of no more than 100 (discretization granularity) meters.

D.2 Additional Results

Table 6: Success Rates of Belief-Averaged DP Pursuers under Different Observation Ranges

Observation Range	2	3	4	5	6
Grid Map	0.78	0.92	0.99	1.00	1.00
Scotland-Yard Map	0.63	0.95	1.00	1.00	1.00
Downtown Map	0.90	1.00	1.00	1.00	1.00
Times Square	0.69	0.88	1.00	1.00	1.00
Hollywood Walk of Fame	0.48	0.79	0.94	0.98	1.00
Sagrada Familia	0.36	0.70	0.92	0.96	1.00
The Bund	0.57	0.87	0.97	0.99	1.00
Eiffel Tower	0.94	0.98	0.99	1.00	1.00
Big Ben	0.74	0.94	1.00	1.00	1.00
Sydney Opera House	0.87	0.96	0.99	0.99	1.00

Table 7: Success Rates of RL Pursuers under Different Observation Ranges

Observation Range	2	3	4	5	6
Grid Map	1.00	1.00	1.00	1.00	1.00
Scotland-Yard Map	0.76	0.98	0.99	0.99	1.00
Downtown Map	0.99	0.99	1.00	1.00	1.00
Times Square, New York	0.95	0.98	1.00	1.00	1.00
Hollywood Walk of Fame, LA	0.38	0.59	0.96	1.00	1.00
Sagrada Familia, Barcelona	0.20	0.72	0.88	0.95	0.96
The Bund, Shanghai	0.25	0.55	0.82	0.82	0.83
Eiffel Tower, Paris	1.00	1.00	1.00	1.00	1.00
Big Ben, London	0.82	0.95	0.98	0.99	0.99
Sydney Opera House, Sydney	0.95	0.98	1.00	1.00	1.00

We may find that Hollywood Walk of Fame, Sagrada Familia, and The Bund are relatively more difficult for the pursuers, especially under small observation ranges. Based on the statistics of the test graphs in Table 1 (left), here we provide a rough analysis of this phenomenon. In planar graphs, a large average degree generally implies the existence of small cycles. For example, in Grid Map, all minimal cycles' length is only 4. Since successful evasions benefit more from large cycles, graphs like Grid Map, Scotland-Yard Map, and Downtown Map are easier for pursuit. Besides, Eiffel Tower, Big Ben, and Sydney Opera House all have large diameters, which implies the existence of long "links" that have poor connectivity with other nodes (see the last three graphs in Figure 5). Therefore, these graphs also benefit pursuit rather than evasion. As Hollywood Walk of Fame, Sagrada Familia, and The Bund do not have the mentioned characteristics, these graphs are harder for the pursuers.

Figure 6 provides the scaling plots of the computation (inference) time of DP and RL policies under an NVIDIA GeForce RTX 2080 Ti GPU, with the log-log plots on the right. Clearly, the time of DP computations significantly increases with the graph sizes. In comparison, the inference time of our GNN-based RL policy is only slightly longer in large graphs than in small graphs.
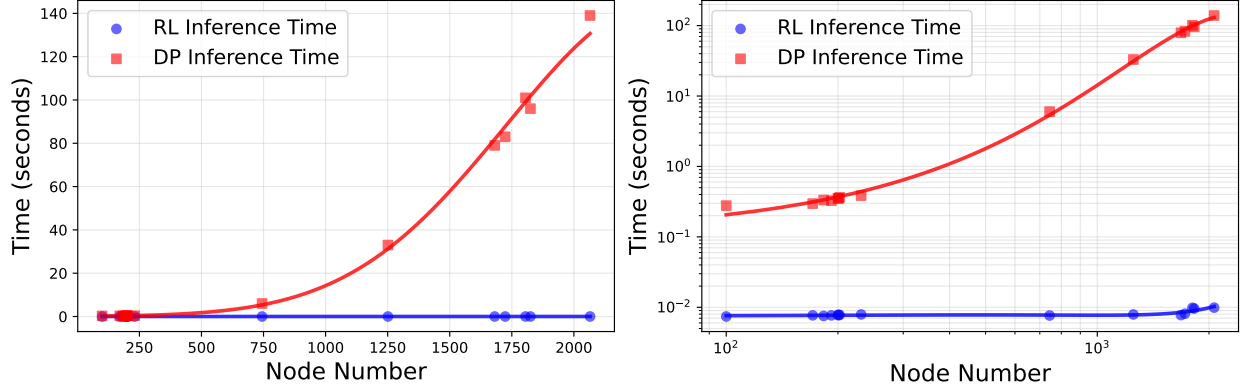
Figure 6: Scaling Plots of RL and DP Inference Time

E   Related Work

Finding optimal strategies in PEGs. Graph-based pursuit-evasion games (PEGs) can be categorized into no-exit PEGs and multi-exit PEGs. The former is the primary form of pursuit-evasion and also the focus of this paper, while the latter is sometimes referred to as network security games. For no-exit PEGs, the early theoretical work Goldstein & Reingold (1995)) proves that it requires exponential time to determine whether m pursuers are sufficient to capture one evader on a given graph under perfect information. (Vieira et al., 2008) provides the provably optimal method for solving sequential PEGs, and (Chung et al., 2011) shows that the basic idea behind PEG solving can be represented by a marking algorithm featuring state expansion. (Horák & Bošanskỳ, 2017) considers the case where the pursuers only have partial observation and provides a dynamic programming algorithm in the form of value iteration for finding Nash equilibrium. (Lu et al., 2025a) shows that an expansion-based dynamic programming algorithm can solve Markov PEGs under a near-optimal time complexity. Recent works (Xue et al., 2021, 2022) combine neural networks with fictitious self-play and Monte-Carlo tree search to construct scalable deep reinforcement learning (RL) algorithms for finding robust pursuit strategies in network security games.

Policy generalization in PEGs. Policy-Space Response Oracles (PSRO) (Lanctot et al., 2017) is a standard game RL paradigm extended from the game-theoretic approach of double oracle (DO) (McMahan et al., 2003) for robust policy learning. While the approach itself is general, it can only solve PEGs on a designated graph structure, just like the methods above. As we have mentioned, policy generalization is crucial to real-time applications under real-world PEGs, becoming a focus of recent research. MT-PSRO (Li et al., 2023) combines multi-task policy pre-training with PSRO fine-tuning to enable few-shot generalization to unseen real-world opponents. Grasper (Li et al., 2024) proposes a two-stage pre-training method to facilitate few-shot generalization to unseen initial conditions of the game. Equilibrium Policy Generalization (EPG) (Lu et al., 2025a) provides a completely novel paradigm to learn generalized policies across the underlying structures of PEGs through the construction of equilibrium oracles, guaranteeing robust zero-shot generalization to unseen graph structures in Markov PEGs. As EPG does not require the time-consuming PSRO tuning, the pursuit strategies are real-time applicable under full observability. However, as is mentioned in Lu et al. (2025a), whether such a kind of generalization can be applied to the case of imperfect information remains unclear. Since partial observability leads to the inherent PSPACE-hardness (see (Papadimitriou & Tsitsiklis, 1987)) and exponentially many information sets (see (Lu et al., 2025b)), constructing equilibrium oracles directly under partial observability can be intractable.